Direct Printing of Lead Zirconate Titanate Thin Films

by

Stephen P. Bathurst

S.B, Massachusetts Institute of Technology (2003)

Submitted to the Department of Mechanical Engineering
in Partial Fulfillment of the Requirements for the Degree of

Master of Science in
Mechanical Engineering

at the

Massachusetts Institute of Technology

February 2008

© 2008 Stephen P. Bathurst
All rights reserved

The author hereby grants to MIT permission to reproduce and to
distribute publicly paper and electronic copies of this thesis document in whole or in part.
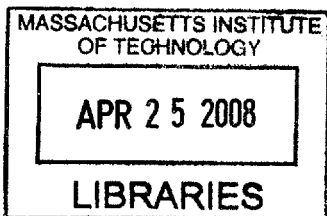
Signature of Author ....
Department of Mechanical Engineering
February 4, 2008

Certified by ....
Sang Gook Kim
Professor of Mechanical Engineering
Thesis Supervisor

Accepted by ....
Lallit Anand
Professor of Mechanical Engineering
Chairman, Committee on Graduate Students

Direct Printing of Lead Zirconate Titanate Thin Films

by

Stephen P. Bathurst

Submitted to the Department of Mechanical Engineering
on February 4, 2008 in Partial Fulfillment of the Requirements
for the Degree of Master of Science in
Mechanical Engineering

ABSTRACT

Thus far, use of lead zirconate titanate (PZT) in MEMS has been limited due to the lack
of process compatibility with existing MEMS manufacturing techniques. Direct printing
of thin films eliminates the need for photolithographic patterning and etching, as well as
allows for controlled deposition over non-planar topographies which cannot be
accomplished with conventional spin coating processes. This thesis reports the optimal
conditions of deposition and crystallization for high dielectric quality PZT thin films via
thermal ink jet printing. Included are details of the solution chemistry developed, printing
conditions required for MEMS quality films, and thermal processing parameters that
enable a strong piezoelectric response.

Thesis Supervisor: Sang Gook Kim
Title: Professor of Mechanical Engineering

Acknowledgments

Table of Contents

List of Figures

Chapter 1.

Motivation and Background

The high degree of piezoelectric and ferroelectric coupling in perovskite phase lead zirconate titanate (PZT) makes it an attractive material for use in microelectromechanical systems (MEMS) [1]-[3]. The piezoelectric coupling coefficients reported for PZT are the largest of all known piezoelectric materials, and as such PZT based devices commonly achieve the highest level of performance [4]. Thin film PZT has been particularly useful in actuator applications because of the much lower operating voltage required than that of the bulk. If the distance between the electrodes of a PZT device is reduced to 1μm or less, usable strain can be achieved with 3V-10V. This voltage range facilitates integration with standard micro-electrical components. Furthermore, the field strength required to permanently align the self-polarizing domains of a PZT film (typically 100V/cm) is easily reached at these operating voltages, removing the need for the high voltage polarization common in bulk PZT applications.

As a result of the strong piezoelectric response and low operating voltage, thin film PZT has been successfully integrated into many MEMS devices. PZT has been used to make arrays of linear actuators that emulate the structure of human muscle [5] and vibration energy harvesters capable of powering wireless sensors and other low power electronics [6]. High performance MEMS resonators, pressure sensors, and pumps that incorporate thin film PZT as the active material have also been demonstrated. Other applications include: nano-positioning stages (such as for a scanning tunneling microscopy), ultrasonic transducers, and MEMS switches. The potential for application of this material cannot be over stated, and the application areas, both imagined and demonstrated, are too diverse and numerous to mention here. PZT has shown itself to be an enabling material, however, the processing of thin film PZT is not easily compatible with the existing MEMS fabrication processes. While challenges remain that must be overcome in order to fully utilize this material in many active MEMS devices, as processing techniques become more compatible with existing MEMS processes, it will continue to add performance and functionality to MEMS in many applications.

Limitations of Current PZT Processing Techniques

The processing of PZT in MEMS has never reached the level one would expect for the most piezoelectric material known. This is due largely to complex manufacturing processing and difficulty in integrating PZT into microdevices. While each of the established PZT manufacturing methods produces films with good dielectric and piezoelectric properties, each method also has limitations that can make integration with MEMS devices difficult.

The non solution based deposition methods, such as sputtering, laser ablation, and chemical vapor deposition, generally require complex and expensive equipment as well as high deposition temperatures. These approaches were developed based on the high volume, bulk processing, manufacturing model relied upon by the semiconductor industry. A cost effective manufacturing model for small volume MEMS applications needs to be developed.

Spin coating, soft lithography, micro-molding, and other chemical solution deposition (CSD) processes, require no vacuum, heating, or complicated equipment for deposition. However, these methods also have process based limitations. While some recent work has demonstrated novel ways of forming sol-gel based films [7], spin coating remains the dominant method of forming the surface gel. Not only is spin coating inherently wasteful of the expensive and difficult to manufacture sol, but it prevents the deposition of PZT films on or around out of plane features. Figure 1 shows the cracking and thinning that occurs when PZT is spin coated over a step about 2μm in height [8].
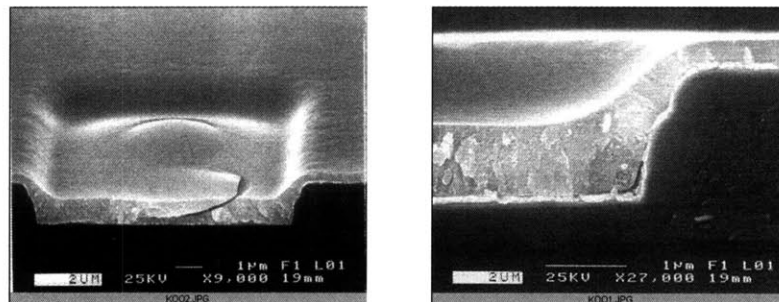
(a) cracking   (b) thinning & high stress

Figure 1. SEM images of spin coated sol-gel PZT films.

9

The sol is also sensitive to other deposition factors, including humidity, particle contamination, and substrate condition and as a result device yields are often low. Reliable deposition requires great care and often a good deal of experience processing PZT thin films. Consequently a flexible new approach is needed to easily and effectively deposit high quality PZT thin films in low volume MEMS applications.

Direct Printing of MEMS

In recent years dot-on-demand (DOD) printing has been studied as a robust, flexible, and inexpensive method of material deposition both for MEMS and for electrical component manufacturing [9]-[10]. While the smallest feature size is currently limited to approximately 25μm, devices for which this resolution is acceptable have been successfully fabricated. Developing a printable ink and establishing the correct printing conditions is a challenge to the printing of any new material, including PZT. It requires careful analysis of many parameters such as: film evaporation rate, substrate interaction, droplet formation, and overall film density and electrical performance. While enabling the reliable printing of a new material can be difficult, previous work has made it clear that, if the relatively poor resolution of DOD printing is tolerable for a particular application, direct printing can provide many advantages over standard manufacturing techniques.

Some of the benefits of DOD printing for MEMS can be summarized as follows. First, no mask or patterning is required. Direct printing enables the designer to deposit a film based on a digital pattern file only. This file can be generated in many ways, including from computer aided design (CAD) software, manually, or based on drawings. Digital deposition in this way eliminates the need for a photolithography and subsequent etching steps in the manufacturing process flow. Furthermore the short cycle time required for pattern generation makes possible rapid prototyping and multiple design iterations that were previously was not possible in MEMS product development.

A further advantage of direct printing is the cost savings due to a reduction in the deposited material consumed during manufacturing and in waste produced. Placement of material only where needed can decrease the amount of material consumed by roughly an

order of magnitude, depending on the device density. This is a significant savings when depositing expensive materials. Manufacturing cost can be reduced further by the removal of the lithography and etching steps. Without lithographic pattering the associated photoresist, developer, etchant, and solvents are all unnecessary as well as the equipment required to coat and expose the substrate. As many of these materials are consider hazardous and required special care during disposal the cost savings can be significant. The result is a manufacturing process that is both cleaner and cheaper than other common deposition techniques.

Perhaps the most compelling benefit of direct printing of MEMS, is that high quality thin films, comparable to spin coated films, can be achieved with deposition control that is not possible with spin coating. Specifically, DOD printing is able to deposit material over and around large out-of-plane features. This makes integration of printing into a manufacturing process flow relatively simple. In addition, the thickness of material deposited can vary deterministically across a device or across a wafer. Thickness can be controlled from tens of nanometers all the way to very high aspect ratio features 100µm tall or thicker [11]. Together, these improvements enable a new geometry of device designs that were previously not possible with simple manufacturing processes. While it is unclear yet what novel devices this new manufacturing method will yield, it is possible that the precise deposition control achieved with DOD printing could have a significant impact on the way MEMS structures are designed in the future.

In order to achieve the potential benefit of direct printing of a new material, three central requirements process requirements must be addressed. First, the ink must print reliably, forming discrete drops without clogging. Second, the geometry of the printed film must be highly uniform and controllable. Finally the properties of the film, both mechanical and electrical, must be predictable and reliable.

Stable printing requires preventing clogging of the printer nozzle during printing, as well as consistent droplet formation dynamics and substrate interaction. Clogging can be caused by particles introduced into the ink during mixing or loading, before printing begins, as well as particles generated during the printing process. Both of these sources must be addressed and controlled. The desired droplet formation and substrate dynamic interaction can be achieved through the careful study of ink, deposition, and substrate

parameters. These parameters include: ink viscosity and volatility, substrate and ink temperature, substrate material, nozzle and droplet sizes among many others.

Achieving film uniformity and resolution acceptable for MEMS devices is also significant challenge associated with drop on demand (DOD) printing. In general DOD printers have been used to deposit material on porous surfaces, constraining droplet spreading and ensuring consistent uniformity. To achieve good results on a non-porous substrate however, the evaporation rate of the ink must be precisely controlled to allow for sufficient spreading of the droplets, but to prevent excessive diffusion of the material in solution.

Figure 2 demonstrates the degree of non-uniformity that is commonly present in DOD printing on nonporous substrates. The figure shows the effect of solute diffusion during film drying for a) discrete droplet deposition and b) a continuous deposited line [12].
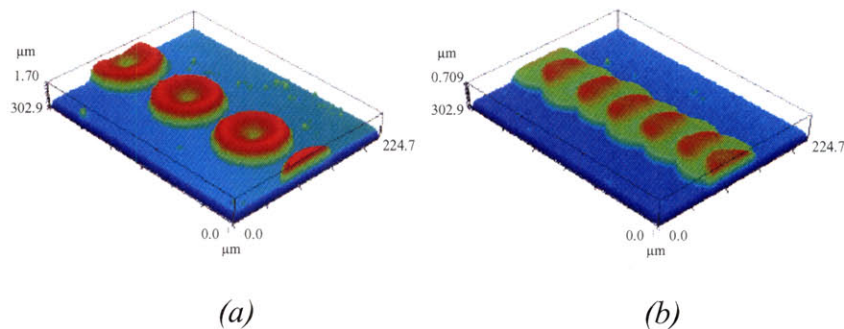
(a)   *(b)*
Figure 2. Non-uniformity in dot on demand printing.

Accurate edge placement is also an important challenge to overcome in direct printing. Achieving the required accuracy, and minimizing variation, requires knowing the degree of spreading, which is a function of the number and placement of droplets, as well as the evaporation rate.

Guaranteeing final properties of a direct printed material requires a technique tailored for each ink and substrate. Many films require special printing environments be maintained or post-processing after printing. Vapor and thermal annealing have been used, as well as laser ablation and chemical process to alter the characteristics of printed films. Almost all of the printing, ink, and substrate parameters can influence the mechanical and electrical performance of a film, and close monitoring of the effect of each parameters effect. Axiomatic Design, developed by Prof. Nam Suh [13], was used

as a tool throughout this research to track the functional interactions, and to ensure that the level of coupling between requirements was minimized.

Ink Jetting of Modified PZT Sol-Gel

This research presents a new method of PZT deposition, based on thermal ink jetting of a modified PZT sol-gel. Previous work has shown the potential of printed PZT through the deposition of paraffin, and ethanol based PZT particle solutions [14]. Rather than a particle based approach, this work attempts to combine the quality of solution based PZT deposition with the flexibility of DOD printing. Printing of a PZT sol-gel based ink has the potential not only to ease process integration manufacturing difficulties, but also to increase the design possibilities for PZT based devices. Producing patterned PZT films directly from digital files will enable rapid design cycles and quick optimization of processing of the films, ensure high quality, high yield deposition. PZT deposition can benefit greatly from the cost advantages provided by direct printing. The sol-gel solutions are difficult to make and often costly (PZT sol-gel costs roughly $100/ml). Finally using ink jet to deposit the sol enables the designer to arbitrarily place PZT between tall features such as electrodes or active structures within a device. This could potentially result in novel actuator or energy harvester designs that are currently not possible.

In order to meet the requirements for reliable printing of thin film PZT, this work focuses on specific solutions to the challenges of ink jet printing of MEMS. The development of stable printing conditions for a PZT sol-gel required determining dilution levels and dynamic analysis of droplet formation. Two methods of achieving acceptable film geometry were developed, one based on printing into a preformed pattern, and one on optimized printing conditions for free formed films. To ensure the PZT film could be annealed into a defect free polycrystalline perovskite phase, a new thermal treatment was determined. Finally, thermal ink jetting of solution based PZT was integrated into a manufacturing process flow and high performance ferroelectric and piezoelectric devices were manufactured. This work reports the first measured piezoelectric properties of printed PZT thin films. It is our hope that this work will be a step towards the robust

production of many PZT based MEMS devices, as well as a tool for producing device designs as yet unseen.

Chapter 2

Piezoelectricity and PZT

In the 1880's Jacques and Pierre Curie discovered that in some materials there is a direct relationship between mechanical strain and electric field. This coupling, known as the piezoelectric effect, allows electrical/mechanical energy conversion in either direction. Mechanical strain within a piezoelectric material induces an electric field. This is commonly referred to as *sensor mode* operation. The application of an electric field causes mechanical deformation, known as *actuation mode*. Piezoelectric materials generally have low maximum strain (typically 0.1%) but high operating frequencies, high maximum force and are very efficient [15].

Polarization and Hysteresis. The electromechanical coupling in piezoelectric materials is caused by an spontaneous asymmetrical charge distribution in the base unit cell of a crystal structure. This charge distribution occurs when ions form a stable, non-center symmetric, structure that has a net charge imbalance, or polarity. When a piezoelectric material is strained, the crystal lattice deforms, and the normal polarization is exaggerated inducing an electric field. Spontaneous polarization is particularly strong in ABO_3 perovskite phase materials such as Barium Titanate ($BaTiO_3$), Lithium Niobate ($LiNbO_3$), and Lead Zirconate Titanate, or PZT ($Pb(Zr,Ti)O_3$. Figure 1 shows a typical tetragonal perovskite structure for a piezoelectric material.
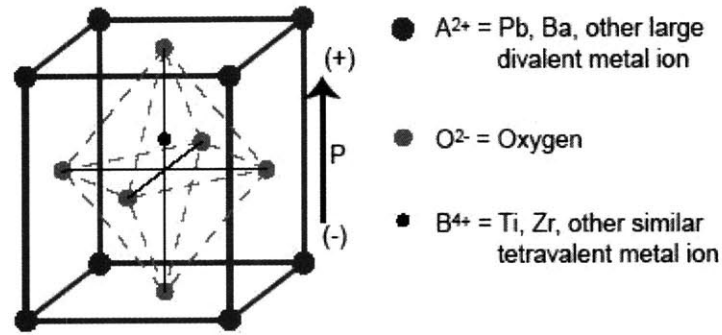
Figure 3. Tetragonal form of perovskite crystal structure [16].

While piezoelectric materials can form single crystal structures, they are most commonly used in polycrystalline form. While each grain in the structure is polarized in a single direction, due to the random arrangement of grains the net polarization of the bulk polycrystalline structure is neutral. In order to form a usable piezoelectric film the polarization of the grains must be aligned by a process known as poling. This is accomplished by applying a strong electric field, under elevated temperature for thicker films, which elongates each grain in the direction of the field. When the field is removed, and the temperature lowered, some permanent realignment of the grains remains. The bulk material is said to be poled, having a bulk net polarization in the direction of the applied field. One of the advantages of thin film piezoelectric devices (thickness <1~2 μm) is that smaller voltages can completely polarize the film at room temperature. Often thin film devices are poled by the field applied during operation. For PZT, the electric field must be on the order of about 100V/cm in order to completely pole the structure, increasing the electric field beyond a critical level, between 40 and 100 V/μm, results in dielectric breakdown of the film.

Due to deformation of the domains under an applied field, the polarization and deflection will lag behind the applied field. This leads to the hysteresis piezoelectric response shown in Figure 4.
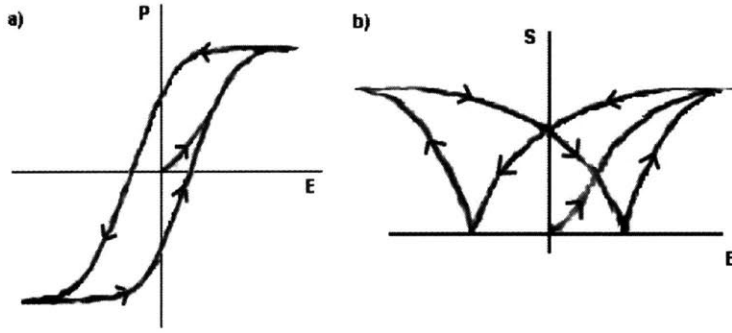
Figure 4. Typical hysteresis of a piezoelectric material in response to an applied electric field a) polarization, and b) strain [17].

The y intercept for the polarization vs. field hysteresis plot is referred to as the remnant polarization. It represents the amount of polarization left over after the electric field is removed and is often used as an indicator of piezoelectric film performance.

Piezoelectric Performance. After polarization, when the applied field is small, the strain is roughly linearly proportional to the applied electric field. The constitutive relationship between electric field and strain of a piezoelectric devices is represented as follows:

$$S_i = s_{ij}^E \cdot T_j + d_{mi} \cdot E_m \qquad (2.1)$$

$$D_m = d_{mi} \cdot T_i + \varepsilon_{mk}^T \cdot E_k \qquad (2.2)$$

The matrices d and s^E contain the material's piezoelectric and compliance constants, based on the directional convention shown in Figure 5, where directions 1 and 2 are in the plane of the piezoelectric material and direction 3 is normal to the film surface.
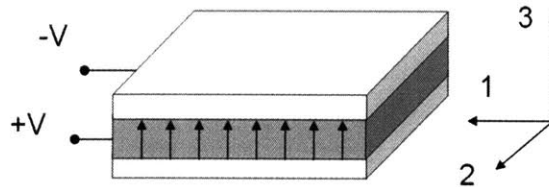
Figure 5. Directional convention for piezoelectric materials [5].

Therefore, the d_{33} constant relates a material's out of plane strain to a parallel voltage field, and d_{31} relates a material's in-plane deflection to a perpendicular filed. Orthogonal

17

deflection in d_{31} mode is not a direct effect of piezoelectricity, but rather a result of the Poisson effect in the directions orthogonal to the applied field and induced strain. Values d33 and d31 values can be difficult to determine and vary widely based on grain size and crystal structure. Table 1 presents some reported constants for common ABO_3 piezoelectric materials. The relatively high values of d33, d31 for PZT indicate that PZT based piezoelectric devices should provide improved performance over those based on other materials.

Table 1: Reported d33 and d31 coefficients for common ABO_3 piezoelectric materials [18]-[21].

Material	d33 $\left[\dfrac{m}{V}\right] \cdot 10^{-12}$	d31 $\left[\dfrac{m}{V}\right] \cdot 10^{-12}$
Lithium Niobate (LiNbO₃)	25	-4.6
Barium Titanate (BaTiO₃)	289	-111.2
Lead Zirconate Titanate (Pb(Zr,Ti)O₃	689	-150

PZT Processing Techniques

The promising properties of thin film PZT have motivated significant work towards developing reliable deposition methods and towards integrating those methods with established planar semiconductor manufacturing processes. The most basic requirements for the successful formation of a piezoelectric PZT thin films include: the deposition of lead, zirconium, and titanium in the correct stoichiometry, and the crystallization of the deposited material into a perovskite phase crystal. Previous work has also shown that controlling grain size is important to achieving a high remnant polarization and coercive field [19]. Finally, for integration into MEMS devices, the deposited film must be sufficiently uniform and patternable. The potential of PZT as an enabling material in MEMS manufacturing has lead to many creative deposition and crystallization techniques that attempt to meet these requirements.

Previously demonstrated techniques for depositing high quality thin film PZT include: sputtering [22], laser ablation [23]-[24], chemical vapor deposition [25], and chemical solution deposition (CSD) processes [26]-[27] . Each of these processes has

been shown to be capable of producing well crystallized PZT films. Table 2 indicates some processing conditions, as well as performance data for each of these deposition techniques.

Table 2. Processing and performance data for common PZT deposition techniques [22]-[27].
Annealing may be required after deposition.

Method	Deposition Temp.* [C]	Deposition Pressure [torr]	Energy Required	Process Complexity	Reported Remnant Polarization [uC/cm2]	Reported Coercive Field [kV/cm]
Sputtering	400-600	$5 \cdot 10^{-3} - 2 \cdot 10^{-4}$	High	High	24	100
Laser Ablation	650-750	$1 \cdot 10^{-4} - 3 \cdot 10^{-4}$	High	High	35	230
Chemical Vapor Deposition	400-800	1 - 760	High	Very High	24	96
Chemical Solution Deposition	Room Temp.	760	Low	Low	26	210

Chemical Solution based films have the most flexibility and are the least expensive and complex of the PZT deposition processes [28]. CSD films are also highly uniform because the reactants can mix at the molecular level while in solution. As a result of these process and quality benefits, solution based methods are currently the most commonly used methods for the deposition of PZT thin films. Sol gel based deposition, a subset of the CSD methods, is by far the most common single method of PZT deposition. A PZT sol is a colloidal suspension of Lead, Zirconium, and Titanium oxides (typically Lead Acetate ($Pb(CH_3CO_2)2\ 3H_2O$), Zirconium-tetra-n-butoxide ($Zr(n-OC_4H_9)_4$) and Titanium-terta-iso-propoxide ($Ti(i-OC_3H_7)_4$)) in a solvent (typically 2-Methoxyethanol). This solution can be spun onto a flat surface and dried, causing the particles to precipitate into a condensed, gel-like, film. The metal-organic gel is then pyrolised into an amorphous stoichiometric mix of metallic molecules. This deposition can be repeated to build films up to several hundred nanometers thick. Finally, after the desired thickness is obtained, the film is annealed into the desired perovskite phase at around 650°C. Sol-gel deposition has proven to be the easiest, cheapest, and most flexible way to form very high quality PZT thin films.

Chapter 3

Thermal Ink Jet Printing System

Thermal Ink Jet Technology (TIPS)

The droplet ejection controller used in this work was the thermal inkjet pico-fluidic system (TIPS). It was developed at HP for printing of functional materials and for use as a flexible development platform. While the design details of the controller and printer nozzles are proprietary technology owed by HP, a review of the basic concepts of thermal ink jet printing based on information available in the public domain is presented here.

The fundamental physics that govern droplet formation in a thermal ink jet printer are based on a rapid pressure increase, caused by the vaporization of a thin layer of ink on a resistive heater, which forces a droplet out through a nozzle. When a pulse of energy is applied to the restive heater, typically 15V-30V for 1-5μs, the heater quickly reaches a temperature greater than 330°C. This rapid temperature increase causes a thin, less than 1μm, layer of ink to vaporize. The vaporization of a small amount of ink causes the internal pressure in the firing chamber to increase to approximately 125atm, which results in droplet ejection. During the thermal event, less than 0.3% of the ink in the firing chamber is heated, and therefore the temperature in bulk ink, when printing at full speed, generally does not rise more than 20°C. Relying on vaporization of the ink for droplet ejection results in non-linear relationship between applied thermal energy and droplet size. Therefore, for a given heater size and nozzle geometry, a relatively narrow range of droplet sizes can be produced. This can be advantageous as it means that slight variations in the printing parameters will be less likely to affect the final printed dimensions. Different size droplets can be produced by using print heads with different nozzle and heater designs, each of which requires slightly different firing parameters. Thermal ink jet printers can commonly operate at frequencies greater than 20kHz and produce droplets that range from 1 pl – 300 pl in volume.

The TIPS controller (Figure 6) provided by HP integrates all of the functions of a full scale thermal ink jet printer into a hand held, or mountable platform. It provides the

ability to control firing pulse parameters and an interface for the replaceable 0.5 ml ink reservoir and print head assembly. It also supplies a connection for regulation of the pressure inside the ink reservoir. A slight negative pressure is required during printing to prevent capillary action from drawing out the ink. Tips with different nozzle sizes and geometries supplied by HP allowed for varied droplet volumes and deposition energy. Finally the TIPS controller provides an interface for computer control and an input for a droplet deposition trigger.
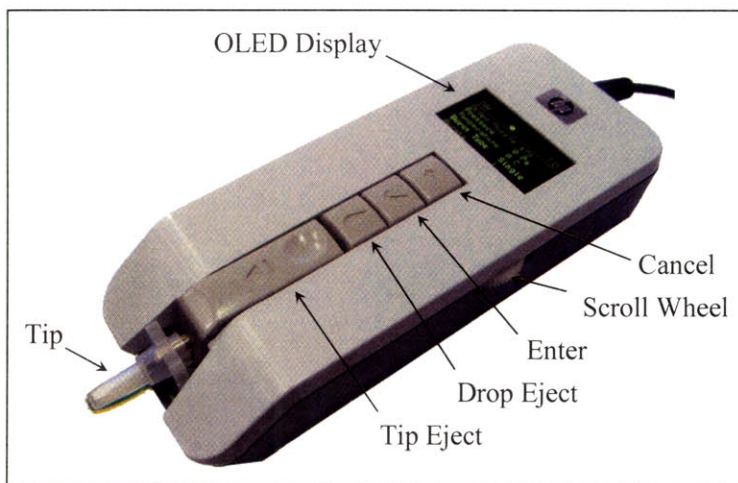
Figure 6. Thermal Ink Jet Pico-Liter System (TIPS) controller. Image courtesy of Hewlett-Packard.

Integrated Printing System (POEM)

An integrated printing system for use with the TIPS controller (Figure 7) was also supplied by HP for this work. The Printing of Electronic Materials (POEM) system was developed as a tool to explore and expand the capabilities of thermal ink jet technology. It has been used to demonstrate the printing of many different materials useful for manufacturing electrical components and MEMS devices. This includes the successful deposition of sol-gel based solutions as well as nano-particle dispersions. It incorporates automated x and y semi-conductor handling stages and a vision system for aligned droplet placement. Printing conditions are set by a digital power controller, a backpressure controller, and a heated vacuum platen. The entire system is controlled by proprietary control software developed by the HP imaging and printing group.

21
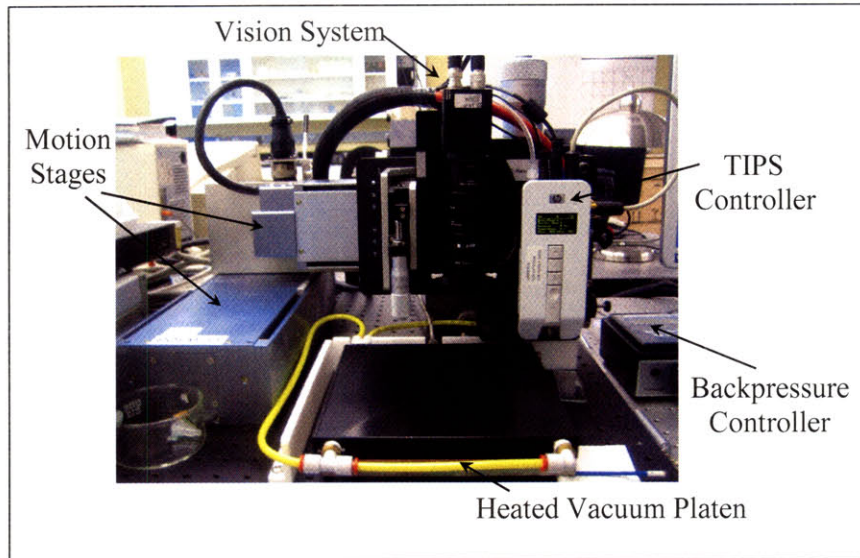
Figure 7. Printing of Electronic Materials (POEM) integrated printing system.

The POEM motion stages are Primatics PLG160 linear stages. They are powered by a ballscrew drive and the position is determined by a 1μm resolution linear encoder. The housing and mountings are aluminum, and all components are compatible with a class 10 clean room environment. With the installed encoder the stages are capable of accuracy ±7.0μm over the 400mm travel range, with repeatability of ±2μm. Motion control is carried out by a Galili DMC-1820 motion controller which interfaces with HP software as well as software developed in the MNSL. The Galil motion controller has built in functions for position and velocity control, as well as auxiliary digital outputs that can be used to trigger droplet ejection. Substrate alignment is accomplished with a CCD camera and video capture card. The video system is used, along with the motion control software, to determine the offset between the camera and the printer tip. Once this offset is established substrates can be aligned to the print head with approximately ±10.0 μm accuracy.

Printer Control Software

Software was developed in the MNSL (Micro Nano Systems Laboratory at MIT) to interface with the motion control card and place drops in a Cartesian coordinate system aligned to a substrate. The software accepts a text file containing sets of coordinates, each

of which represents a droplet location. Alignment is accomplished based on the position of two alignment marks set by the user. The position of the two marks enables the calculation of the center of the substrate as well as the angular misalignment. Based on the location of the substrate an offset is determined for each droplet, and new droplet coordinate calculated. In this way all droplet locations are transferred into the substrate coordinate system and the device layer to be printed is aligned.

Tools were developed using Matlab® to facilitate the generation of input patterns based on certain user specified parameters. For example, starting and ending locations were used to generate close packed area coverage patterns. Droplet spacing and an edge offset were also variable parameters that could be specified by the user. Droplet spacing was generally used to control film thickness, and the edge offset was used to ensure that, after spreading, the edge of the printed line was in the correct location as specified by the start and end points. The software was structured in this way so that the pattern generating code would closely represent the functional design intent. This allowed printing conditions to be changed without having to recreate the entire pattern manually. The result was the ability to rapidly generate new pattern files for a given droplet size and set of printing conditions, as long as the appropriate line edge offset and droplet spacing had been previously determined. Figure 8 shows a plot of a device layer pattern generated in Matlab®. Once the appropriate pattern is generated, and the substrate is aligned, a printed layer can be easily integrated into either a fully printed process flow or one which incorporates standard lithographically processed layers.
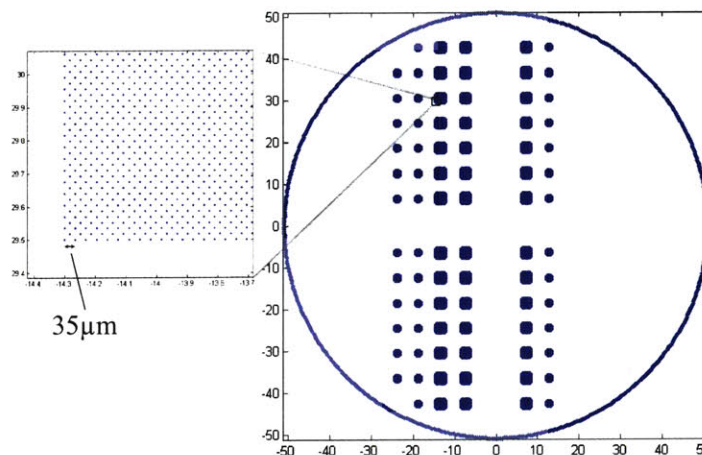
Figure 8. Matlab® plot of a typical printed device layer pattern.

Chapter 4

Ferroelectric Capacitor Design and Fabrication

A ferroelectric capacitor was designed and built to test the electrical properties of the printed PZT films. With the exception of the printed PZT layer, all processing methods were based on well characterized MEMS techniques. The electrodes of the capacitor were deposited and patterned using the same process parameters previously used to grow high quality PZT thin films with a sol gel method [5]. To allow for less precise edge formation with ink jet printing, electrode mask patterns were designed with the maximum possible margin for error. Due to the uncertainty of substrate alignment and positional accuracy of the motion stage during printing, each mask layer incorporates devices that are able to accommodate a range of misalignment from 100 μm up to 1 mm in both x and y axes. The size of the bottom electrode ranges from 0.0121 cm^2 to 0.09 cm^2 to allow for testing of different printed areas. Similarly, capacitor size is varied through changing the area of the top electrode, which ranges from $2.5 \cdot 10^{-5}$ cm^2 to 0.01 cm^2. Details of the mask designs can be seen in Appendix A: Ferroelectric Capacitor Masks. The device design was intended to facilitate both the development of the printing process and comparison with well understood deposition methods for PZT.

Device Structure

All of the devices were manufactured on standard P-type <100> 4" silicon wafers. Silicon is a common substrate for PZT growth because of its ability to handle the high annealing temperature and its inherent compatibility with all semi-conductor processing techniques. The bottom electrodes of the capacitors were titanium and platinum, which are common PZT seed layers. Electron beam evaporated, or sputtered, platinum is used as a seed layer because it promotes the growth of [111] oriented perovskite phase PZT crystals when annealed. A thin layer of titanium (approximately 20 nm) serves not only as an adhesion layer for the platinum, but also helps the growth of high quality PZT. Previous work has shown that the growth of PZT is aided by the diffusion of titanium up

through the platinum seed layer [29]. To encourage the diffusion of titanium, each wafer was covered with thermally grown silicon dioxide of thickness between 170nm and 200nm before the bottom electrode deposition. The oxide layer acts as a diffusion barrier to ensure the titanium only diffuses upward, and lead does not diffuse down into the substrate. It has been shown that a silicon dioxide layer thicker than 100 nm will provide an effective barrier [30]-[31]. A cross section of a typical device structure can be seen in Figure 9.
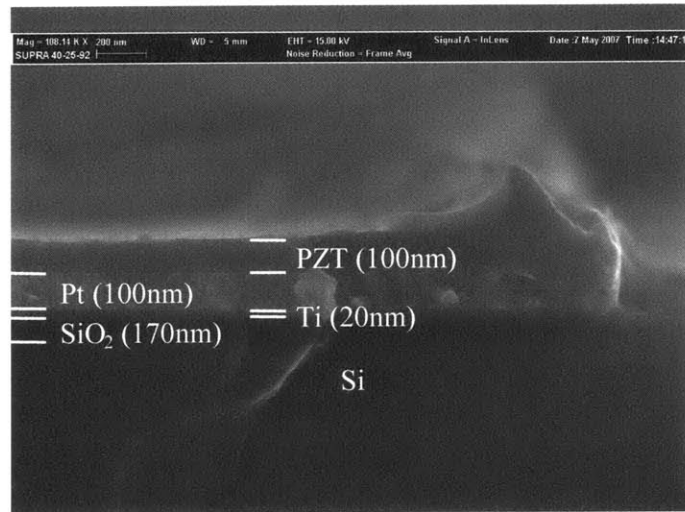
Figure 9. Cross section of a ferroelectric capacitor with a thermal ink jetted PZT layer. Device is shown without a top electrode

Process Overview

Two ink jet printing processes were developed to determine the resolution limits and electrical performance of PZT printing. The first process utilizes a PZT film that is printed freely onto the platinum substrate which relies on surface tension and evaporation rate to determine the printing resolution and uniformity. The second involves the patterning of a mold into which the PZT ink is printed. The purpose of developing two processes was to see what improvement in printed geometry would be achieved by printing the PZT with a mold. Mold-printed PZT has a uniform, clean-edged geometry and can therefore be compared with free printed films to determine the effect of geometry on the film properties. Both designs have electron beam evaporated top and bottom

electrodes patterned with image reversal and liftoff. The molded PZT process uses a pattern made from 300 nm thick electron beam evaporated polysilicon, etched with a XeF_2 dry etch, to form the molds. Detailed processing plans are included in part one of Appendix B: Ferroelectric Capacitor Process Plans.

Design Improvements

Over the course of developing the capacitor, certain design changes were made in order to improve the printed device performance. The top electrode pattern was changed, as was the photoresist used to form the pattern, and finally the thickness of the platinum layer was increased. Each of these changes had a noticeable impact on the sensitivity of manufacturing process and hence the device yield.

The first of the changes made was in the design of the top electrode pattern. In the early iterations of the device, the top electrode area was matched to that of the bottom electrode, minus the X,Y misalignment tolerance. In initial tests with this design, many of the larger devices had shorts between electrodes. Defects appeared with roughly constant area density for a given set of printing conditions. Therefore the larger area devices were more prone to defects and cracks. However, printing larger area capacitors was desirable because the printing conditions were more reliable. Large area devices allow the use of larger nozzle sizes, are less sensitive to PZT ink chemistry, and have a greater misalignment tolerance. The redesign of the top electrode includes many small capacitors on one large bottom electrode seed layer. This allows for large area printed deposition with smaller device structures as well as it allows for easy wiring of top electrodes to test two devices in series.

(a) Version 1   *(b) Version 2*
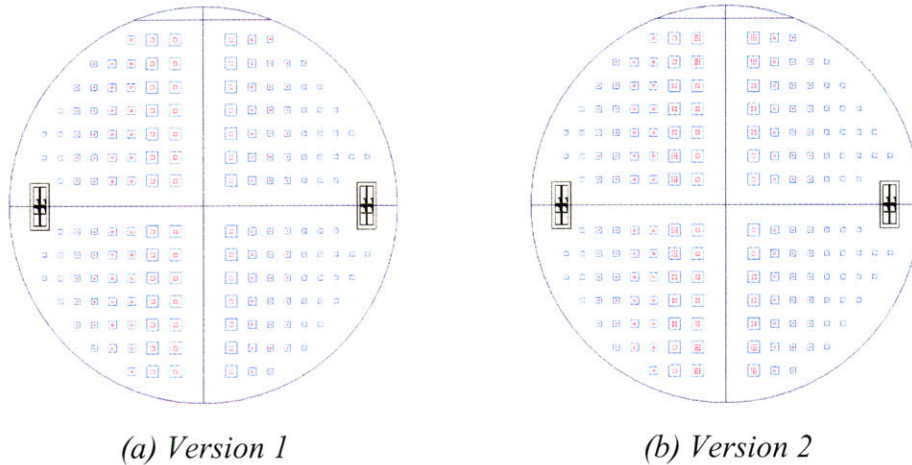
Figure 10. Comparison of the two fabricated top electrode designs (pink). Both are overlaid with the bottom electrode for reference (blue).

The next design change made during the processing of the ferroelectric capacitor was an increase in the thickness of the platinum seed layer. The original device design has 100 nm thickness of platinum. This thickness was the same thickness used in other PZT MEMS work in our group, and was chosen to facilitate comparison with similar devices. Initial tests with this thickness showed serious hillocking, after the annealing of the PZT, that rendered the devices unusable. The hillocking was also present in other PZT based devices processed in the MNSL with the same device structure (Figure 11).
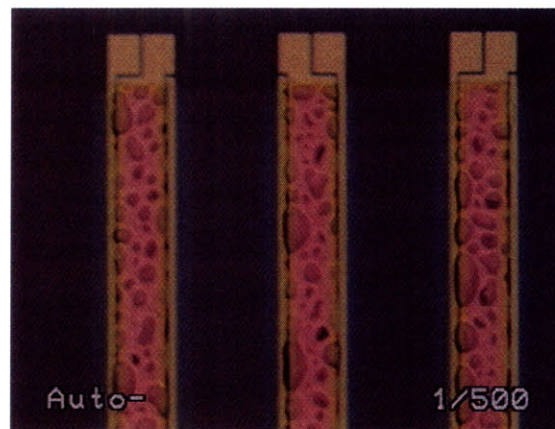
Figure 11. Hillocking of 100nm of platinum on 20nm of titanium. The damage to the PZT resulted in shorted, unusable devices [5].

27

Research into previous work suggests that hillocks in Pt/Ti electrodes form during the release of compressive stress and recrystallization of platinum during annealing [32]. It further indicates that thicker platinum can better resist the high temperatures and will mitigate the hillocking. As a result, the thickness of the deposited platinum was increased to 200 nm. This resulted in a significant improvement in device yield and hillocking of the platinum was no longer an issue.

The final process change was the selection of the photoresist used to pattern the electrodes. AZ-5214 produced by Clariant was the photoresist initially used for the image reversal pattern formation prior to metal deposition. Significant problems were experienced with the use of AZ-5214, and reliable results were never achieved. It is highly sensitive to humidity, and thus exposure and develop times can vary wildly in our humidity prone fabrication facility during summer. Furthermore AZ-5212 is a positive photoresist that requires two well characterized exposures in order to achieve reliable image reversal results. These devices were formed based on transparency masks which can easily become dirty or damaged, distorting the image. As a result it is highly desirable to have a robust photoresist that can accommodate mask imperfections. Based on recommendations from others performing image reversal processes, the photoresist was changed to NR7, manufactured by Futurrex. NR7 is a true negative photo resist requiring only one exposure with a wide range of acceptable exposure and develop times. Once the process was changed to NR7 and device electrode resolution and yield were both improved. It is still however recommended that chrome masks be used whenever possible for image reversal. Details of the NR7 based process plans are included in part two of Appendix B: Ferroelectric Capacitor Process Plans.

Chapter 5

Results and Discussion

The development of stable printing conditions for a PZT sol-gel, controlling film geometry, and crystallization of the printed film into a defect free polycrystalline perovskite phase were the central focuses of the experiments and analysis of this research.

Printing Consistency and Reliability

All of the PZT inks for this work were based on Mitsubishi A6 50/49 PZT sol-gel. Combinations of 2-methoxyethanol, isopropanol, and 2-ethylhexanoic acid were added to the sol to dilute the inks. 2-methoxyethanol is the solvent used in the manufacture of the sol-gel and helps control hydrolysis of the metal organic molecules. 2-propanol is a common mild solvent with a low boiling point that is known to be reliable in thermal inkjet printing. Finally 2-ethylhexanoic acid was to control overall ink volatility as it has a high boiling point and is also known to be compatible with thermal ink jet.

To prevent clogging of the printer nozzle, three sources of particle contamination were addressed and controlled. First, to eliminate external particle contamination each ink was filtered with a 0.45μm PTFE syringe filter and deposition was carried out in a hermitically seal glove box filtered with 99.99% efficient removal of 0.2 micron and larger airborne particles. Figure 12 demonstrates the improve particle control that was achieved by implementing these filtering measures.
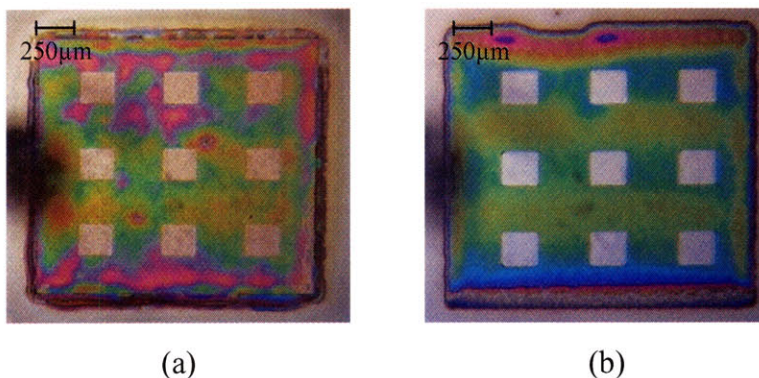
Figure 12. Film quality observations taken a) before and b) after the implementation of particle control measures

Particle formation during the printing process was also a concern due to the decomposition of the metal-organic molecules during the thermal event. Throughout this work over thirty ink chemistries, with dilution levels ranging from the as purchased 15%wt of metal oxides down to 2%, were tried and empirically the appropriate levels of dilution were observed. Table 3 shows observations of the concentration required for reliable printing for different nozzle sizes.

Table 3: Maximum allowable metal oxide concentrations for reliable printing of different droplet sizes.

Droplet Volume (pl)	Maximum Acceptable Concentration (%wt)
180	15
80	4.7
35	2.3

Finally, preventing clogging requires controlling the evaporation rate of the ink such that a stable meniscus is formed at the nozzle. If the solvent evaporates too quickly, metal oxide particles are built up inside the nozzle and firing chamber and result in concentrations that exceed stable printing requirements. This was prevented by printing continuously to maintain a constant ink follow through the nozzle.

To ensure predictable substrate wetting and stable droplet formation, certain dimensionless numbers known to govern drop on demand printing dynamics were calculated and observations were made to ensure the accuracy of the predicted results. The forming of a film on the substrate is characterized by the Bond number, which for these droplet sizes will be no larger than approximately $4 \cdot 10^{-3}$ (see Appendix C Part 1:

Calculation of Bond Number for Film Formation Analysis). As for most ink jet printing, the Bond number for this work is sufficiently low to ensure the film shape on the surface will be dominated by surface tension, forming spherical caps for single drops and cylindrical slices for a printed line. Figure 13 shows an image of a spherical cap of 2-methoxyethanol forming on a platinum substrate during contact angle measurements. The contact angle was measured between 10°-12°, although accuracy can not be guaranteed for measurements at such low angles.

Figure 13. Advancing contact angle measurements of 2-methoxyethanol on platinum.

Previous work has shown the ratio of the Reynolds number to the square root of the Weber number dictates the dynamics associated with droplet formation [33].

$$Z = \frac{(\gamma \rho a)^{1/2}}{\eta} = \frac{Re}{We^{1/2}}$$

Most DOD inks have $1 < Z < 10$. Viscous dissipation can prevent droplet ejection for $Z < 1$ and for $Z > 10$ multiple drops, or even a constant stream, can result. Appendix C Part 2: Calculation of Z for Droplet Dynamic Analysis, gives details on an estimate of the range Z values expected for this work, between 1 - 40. The nominal value of the sol-gel based ink is approximately 20-25 which is slightly higher than is ideal for dot-on-demand printing, and indicates a high probability of stream and satellite droplet formation. However, reliable DOD printing has been shown for higher Z values, and discrete droplet formation was observed at low frequencies and for the smaller nozzle sizes. Therefore, while the high value for Z indicated a need for close monitoring of droplet formation, because stable droplet formation has been demonstrated for these values of Z, and was observed in this work, Z value was never a primary design driver.

Control of Film Geometry

This work characterized the resolution limits of two methods of printed PZT patterning. The first involved printing into a predefined mold and the second, free printing method, was based only on droplet size and wetting angle with the substrate. Printing into a mold to pattern the PZT removes the coupling between pattern resolution and film uniformity that occurs due to the dependence both have on film evaporation rate. When using a mold, droplet spreading and solute diffusion are controlled. Therefore the evaporation rate can be very low, allowing for highly uniform films without a loss of resolution. Figure 14 demonstrates the resolution achieved for cast PZT films.
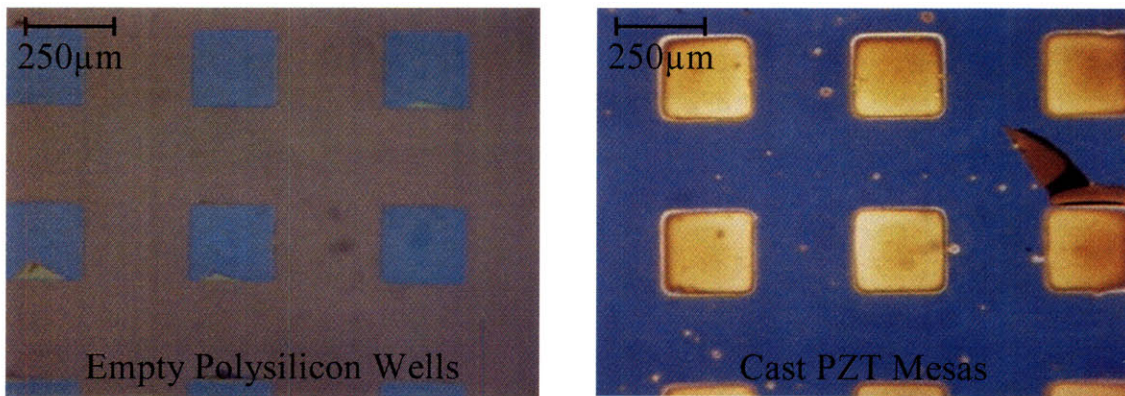
Figure 14. Results of thermal ink jet printing of PZT into preformed polysilicon molds.

Surface profilometry was used to characterize the step definition and the roughness of the cast PZT films (Figure 15). Edge effects were clearly visible on all samples due to wetting of the PZT ink to the side walls of the mold. This however, was not a concern because it can be controlled by adjusting the height of the mold to match that of the desired PZT film. In general the geometry of the PZT films printed into lithographically pattern molds was controlled to the accuracy of the mold itself. Uniformity was also very good: for a printed film with a bulk mean thickness of 147 nm the RMS roughness was 9 nm.
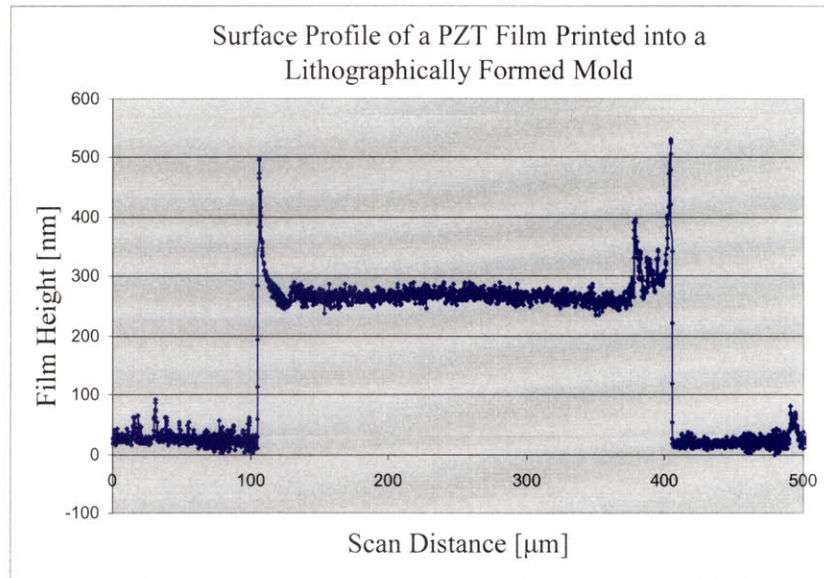
Figure 15. Profilometry of PZT film printed into a preformed mold.

Mold-free printing for MEMS is attractive because the mold removing step after printing adds complexity to the process. However, printing without a mold makes it more difficult to achieve the geometric control required. The diffusion of solutes towards the film edges during solvent evaporation known as the coffee stain effect can lead to significant non-uniformity [34]. Figure 16 shows how early printed PZT films exhibited this effect. In order to overcome this non-uniformity a study was conducted to determine the ink volatility and substrate temperature required to achieve the optimum level of spreading and diffusion. This can be eliminated also by multiple layer printing.
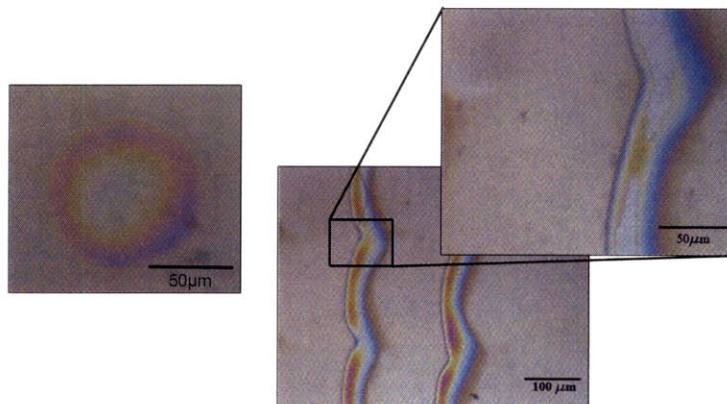
Figure 16. The influence of the coffee stain effect on dot on demand printing of PZT.

Controlling uniformity of free printed PZT films requires controlling the amount of diffusion of the metal oxides towards the film edges that can occur as the volatile solvents are evaporated. It was observed that ink chemistries with an excess of 2-methoxyethanol always exhibited significant metal oxide diffusion, and therefore non-uniformity. Given the relatively high levels of dilution required, isopropanol was selected to make up the bulk of the ink given that it had a lower boiling point and would evaporate more quickly controlling diffusion of the oxides. It was found that inks that were made up of 50 % isopropanol and 15 % PZT Sol would both print reliably as required by the clogging constraints, and evaporate quickly enough to prevent significant diffusion.

To achieve highly uniform films, precise control over evaporation rate is required. This is accomplished by adjusting the substrate temperature. However, the range of substrate temperatures available is limited to approximately 70°C to prevent clogging as a result evaporation of ink from the printer nozzle. Due to this limit on substrate temperatures it is desirable to control the volatility of the ink to ensure that the desired evaporation rate can be achieve within the given temperature range. This was accomplished using the remaining 35 % of the ink which was comprised of a mixture 2-methoxyethanol and 2-ethylhexanoic acid. The boiling point of ethylhexanoic acid is significantly higher than the other solvents (228°C), and therefore the concentration of ethylhexanoic acid was used to control the overall ink volatility, with anhydrous 2-methoxyethanol making up the remainder of the ink. Figure 17 demonstrates the control over film geometry that is possible by adjusting the substrate temperature, when the ink volatility is set to an acceptable level.
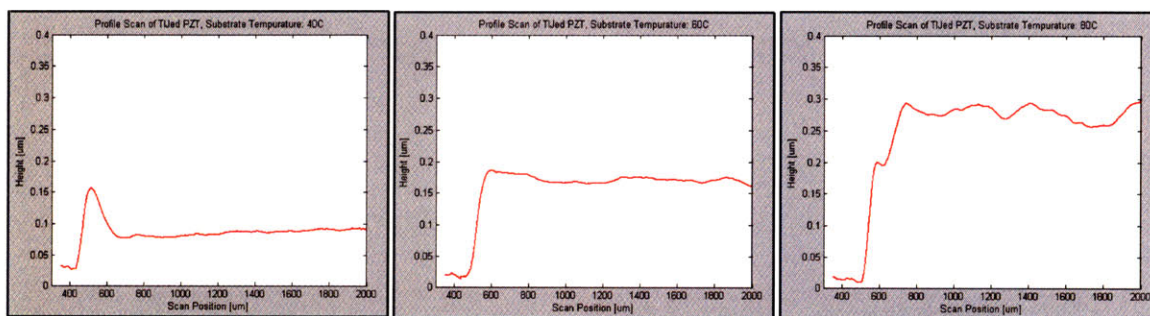
Figure 17. Profilometry of thermal ink jetted PZT, deposited at different substrate temperatures. Ink composition: 6% EHA, 15%PZT, 50%IPA, 29%ME.

In is clear from the profilometry data that if the deposition temperature is too low the metal oxide solutes diffuse to the film edge and accumulation occurs. However, if the deposition temperature is too high, the solvent evaporates before each droplet has a chance to fully merge with neighboring droplets, resulting in residual surface texture from the initial droplet shapes. In order to determine the optimal substrate temperature for this ink (6% EHA, 15%PZT, 50%IPA, 29%ME) 15 samples were prepared at different temperatures (Figure 18).
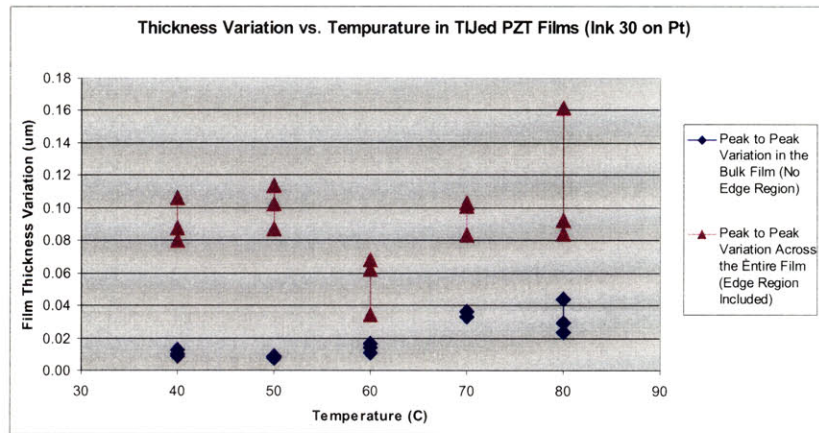
Figure 18: Study 1 of thickness variation vs. substrate temperature for thermal ink jetted PZT on Pt. Ink composition: 6% EHA, 15%PZT, 50%IPA, 29%ME.

The results of the study clearly showed an optimum deposition temperature at 60°C. However, to ensure that clogging of the nozzle due to excessive solvent evaporation would not be a problem, it is desirable to reduce the substrate temperature during deposition. A new ink was prepared made up of 5% EHA, 15%PZT, 50%IPA, 30%ME, and the study was conducted again. Figure 19, shows the results of the second uniformity vs. substrate temperature study, which show a reduction in optimum deposition temperature from 60°C to 50°C. Together these two studies demonstrate the effectiveness of using substrate temperature to control deposition uniformity, and using ink volatility to ensure that the substrate temperature doesn't violate clogging constraints.
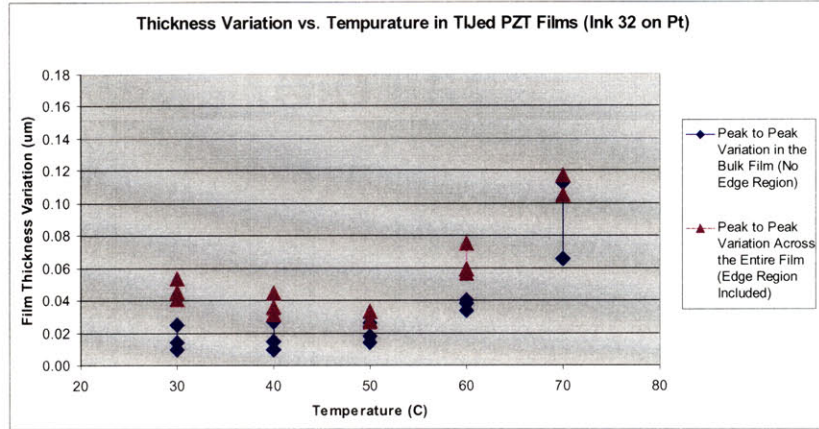
Figure 19: Study 2 of thickness variation vs. substrate temperature for thermal ink jetted PZT on Pt. Ink composition: 5% EHA, 15%PZT, 50%IPA, 30%ME.

Crystallization of Printed PZT Thin Films

There are three steps required to properly crystallize a sol gel based PZT thin film into a piezoelectric, perovskite phase. The first is the drying of the solvent in which the metal organics are dissolved. The second is the decomposition of the metal organics into an amorphous film. Finally the film must be annealed into a perovskite structure. The thermal processing of the early printed PZT films was determined based on manufacturer's recommendation and experience in processing spin coated films of the Mitsubshi A-6 50/49 PZT sol gel. The details of the initial thermal processing can be seen in Table 4.

Table 4: Thermal processing conditions for spin coated PZT thin films.

Processing Step	Temperature [°C]	Time [min]
Dry – Solvent Evaporation	260	3
Pyrolysis – Decomposition of Metal Organics	360	8
Anneal – Crystallization	650	20

With the same thermal treatment made on the printed PZT shows very poor piezoelectric performance (see Figure 22.a) and low film resistivity. At 5 V the film resistivity measured was $4.5 \cdot 10^{10}$ $\Omega \cdot cm$, however at 15V the resistivity dropped to $8.3 \cdot 10^2$ $\Omega \cdot cm$ which is far too low to be useful for a MEMS device. For a full summary of film properties see Appendix D. Performance Data Summary for Thermal Ink Jetted PZT.

Previous work indicates that amount of decomposition of the metal organics strongly affects the crystallographic phase transition, and therefore piezoelectric performance [35]. The poor piezoelectric performance was therefore attributed to incomplete pyrolysis, likely due to the dilution of the PZT sol-gel for jetting. With heavy dilution, and the addition of higher boiling point solvents, the solvent evaporation was incomplete after 3 min at 260°C. The solvent remaining in the film prevented the required decomposition of the organics during the subsequent pyrolysis step which lead to the poor film properties.

In order to achieve improved piezoelectric performance, the drying step was lengthened to try and ensure complete evaporation of the solvent prior to pyrolysis. FTIR analysis was performed on two samples dried 260°C for 2hrs, one in air and one under vacuum. Both samples showed a small reduction in the absorption peaks associated with the added solvents (Wavenumbers [cm^{-1}] 2954, 2923, 2873, and 2852). To remove the remaining organic material, Pyrolysis time was also increased to 2hours, after which FTIR analysis showed the removal of nearly all of the organic material (Figure 20).
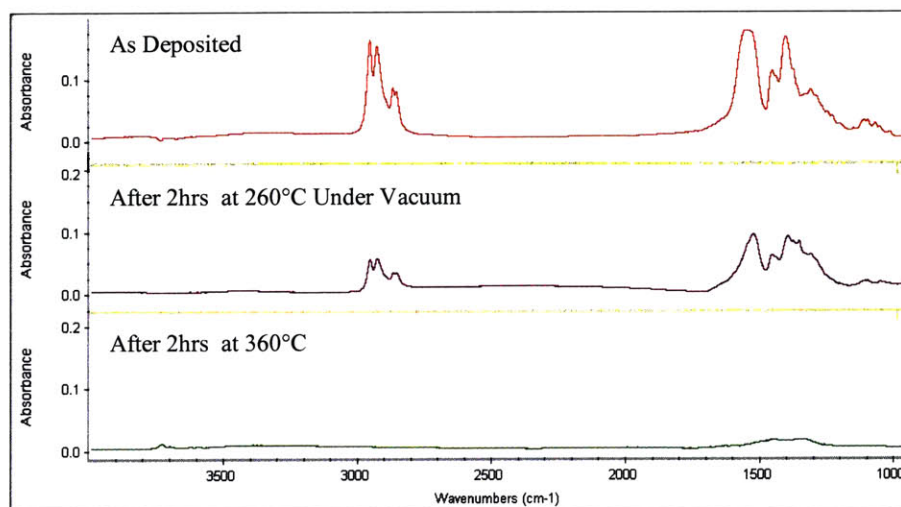
Figure 20: FTIR of a printed PZT thin film during heat treatment.

The final change in thermal processing was a reduction of the annealing time. Previous work has shown smaller grain sizes results in higher performance films [19]. The annealing was therefore performed in a rapid thermal anneal system for 2min to reduce the resulting grain sizes. The details of the updated thermal processing can be seen

in Table 5. After finalizing the thermal processing conditions, X-ray diffraction was used to confirm the crystallographic structure after annealing. The film was shown to be pure perovskite phase with no pyroclore present (Figure 21).

Table 5: Thermal processing conditions for thermal ink jetted PZT thin films.

Processing Step	Temperature [°C]	Time [min]
Dry – Solvent Evaporation	260	120
Pyrolysis – Decomposition of Metal Organics	360	120
Anneal – Crystallization	650	2
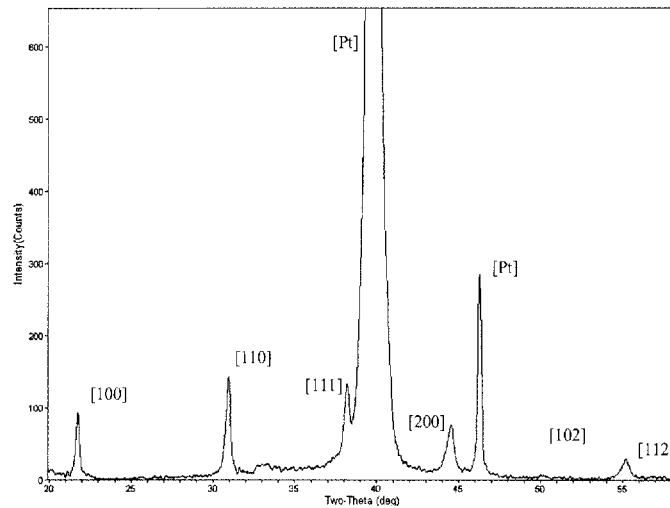
Figure 21: X-ray diffraction of a printed PZT film. All peaks are associated with the perovskite phase, no pyroclore is present.

Under this new thermal treatment the dielectric properties of the films were significantly increased. At 5V the film resistivity measured was $6.4 \cdot 10^{10}$ $\Omega \cdot$cm, and at 15V the resistivity was still to $6.2 \cdot 10^{10}$ $\Omega \cdot$cm. The results of the polarization voltage hysteresis curve can been seen in Figure 22.b. As compared to a spin coated film the remnant polarization is still lower than desired, but with the improved dielectric performance the printed film has met the minimum requirement for successful MEMS device operation.

Figure 22: Polarization vs. voltage hysteresis curve for a thermal ink jetted PZT thin film a) after standard pyrolysis and b) after extended pyrolysis as well as c) for a spin coated film after standard pyrolysis.

Chapter 6

Conclusion

A new solution based PZT deposition method has been developed that provides increased flexibility and lower manufacturing costs over standard deposition methods. Ink chemistry that can be reliably jetted has been developed; printing conditio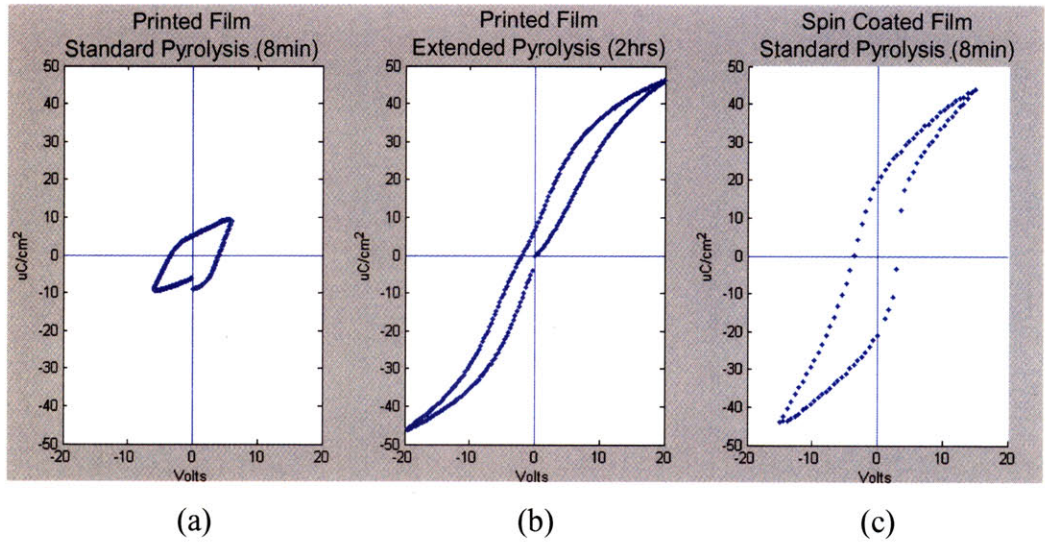ns are determined; the appropriate thermal processing parameters are characterized to ensure a perovskite phase after annealing. This required implementing particle control measures, determining the right amount of dilution required to control particle formation, and ensuring minimal evaporation from the printer nozzle.

Analysis was performed on droplet formation dynamics and on substrate wetting conditions. A method for determining the optimum deposition temperature for dot on demand printing of highly uniform thin films on a nonporous surface was presented. Furthermore, a method for creating and using cast features as mold for thin film deposition was developed. Printing of cast films was demonstrated to have significantly improved resolution and uniformity over standard drop on demand deposited films.

Finally the thermal processing conditions were determined for the annealing of printed PZT films into pure perovskite phase poly crystalline films. Pyrolysis time was investigated as a means for controlling film crystallization. Fourier transform infrared spectroscopy was used to confirm the complete removal of the organic material in our highly diluted PZT ink and X-ray diffraction was used to confirm the final crystal phase.

Taken together these results provide a new method of depositing PZT that makes current processing easier and robust while simultaneously enabling device designs that were not previously possible. It is likely that the solution chemistry and deposition conditions developed in this work will translate directly to the printing of some of the numerous other sol-gel based materials. The method of achieving highly uniform free printed films has the potential to significantly improve the mechanical and electrical properties of many printed films, and may enable the printing of new materials highly sensitive to thickness variation, as is the case for PZT, while the casting based patterning may provide a new way to achieve the levels of performance common in the semiconductor industry via printing.

Future Work

While this new printing method shows great promise, there is still much work to be done. First and foremost the remnant polarization of the printed films is still only about one quarter of those processed via standard sol-gel processing methods. Crystallization of sol-gel based PZT has been analyzed and optimized over the last thirty years, so it is not surprising that a new solution chemistry would have a slightly reduced piezoelectric response. Film purity, density, and grain size are all closely related to the heating cycles that the film undergoes. With better understanding of the effects of the thermal processing, performance similar to spin coated films should be achievable.

The final measure of the quality of a piezoelectric film are the d33, d31 coupling coefficients and printed films should be tested. This requires the integration of a printed film into an active device structure, such as a cantilever of diaphragm. This requires only slight improvements to substrate alignment and deposition accuracy, largely dependent on the resolution limits of the integrate vision system, and work in the MNSL to fabricate a printed active devices is currently underway.

Finally, printing of PZT onto other substrates should be investigated. Platinum seed layers are common for actuators, but often zirconium oxide is used as a seed layer for sensor or energy harvester devices with the d33 mode design. Zirconium oxide is also available in a sol-gel form and it is possible that the solution chemistry developed will enable at multi-layer or even a fully printed set of devices. It is the hope of the author that this work will contribute to the growing field of printed MEMS and electronics in a way that helps this promising method achieve the level of quality that will enable a substantial positive change in the way devices are designed and produced.
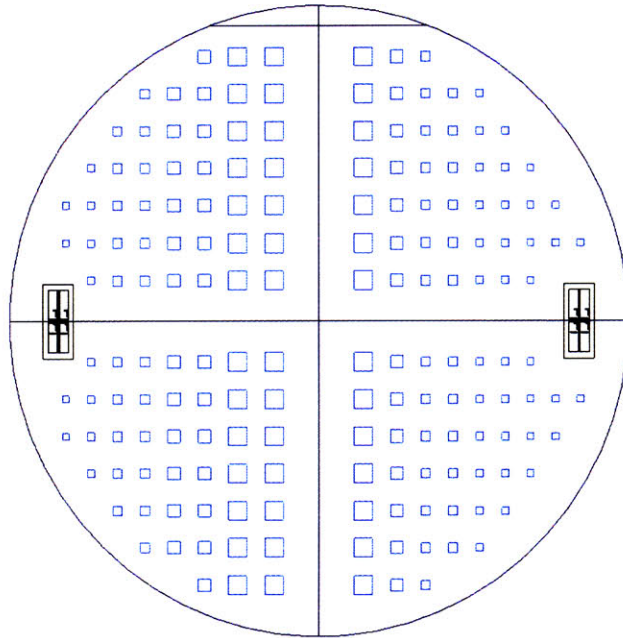
References:

[1] Y.C. Hsu, C.C. Wu, C.C Lee, G.Z. Cao and I.Y. Shen, "Demonstration and characterization of PZT thin-film sensors and actuators for meso- and micro-structures," Sensors and Actuators A, vol. 116, pp. 369–377, May 2004.

[2] W.J. Choi, Y. Jeon, J.H. Jeong, R. Sood, and S.G. Kim, "Energy harvesting MEMS device based on thin film piezoelectric cantilevers," Journal of Electroceramics, vol. 17, pp. 543–548, November 2005.

[3] S.J. Gross, S. Tadigadapa, T.N. Jackson, S. Trolier-McKinstry, Q. Q. Zhang, "Lead-zirconate-titanate based piezoelectric micromachined switch," Applied Physics Letters, vol. 83, no. 1, pp. 174-176, July 2003.

[4] P. Muralt, "PZT Thin Films for Microsensors and Actuators: Where Do We Stand?" Ultrasonics, IEEE Transactions on Ferroelectrics and Frequency Control, vol. 47, pp. 903-915, July 2000.

[5] Z. Traina and S.G. Kim, " A Large Strain Piezoelectric Microactuator by Folding Assembly," M.S. thesis, Massachusetts Institute of Technology, Cambridge, MA, 2005.

[6] R. Sood and S.G. Kim, "Piezoelectric Micro Power Generator (PMPG): A MEMS-Based Energy Scavenger," M. Eng. thesis, Massachusetts Institute of Technology, Cambridge, MA, 2003.

[7] C. R. Martin and I. A. Aksay, "Topographical Evolution of Lead Zirconate Titanate (PZT) Thin Films Patterned by Micomolding in Capillaries," Journal of Physical Chemistry, vol. 107, pp. 4261-4268, January 2003.

[8] S.G. Kim and M.K. Koo, "Design of a microactuator array against the coupled nature of microelectromechanical systems (MEMS) processes", in Annals of the CIRP, vol. 49, no. 1, 2000.

[9] S. B. Fuller, E. J. Wilhelm, and J. M. Jacobson, "Ink-Jet Printed Nanoparticle Microelectromechanical Systems," Journal of Microelectromechanical Systems, vol. 11, no. 1, February 2002.

[10] C. M. Hong and S. Wagner, "Inkjet Printed Copper Source/Drain Metallization for Amorphous Silicon Thin-Film Transistors," IEEE Electron Device Letters, vol. 21, no. 8, August 2000.

[11] R. Noguera, C. Dossou-Yovo, M. Jejeune, and T. Chartier, "Fabrication of 3D fine scale PZT components by ink-jet prototyping process," Journal de Physique IV, vol. 128, pp. 87-93, 2005

[12] D. Gamota, "Crossing the Chasm: Commercializing Printed Electronics," presented at A United States Measurement System Workshop: Large-Area, Flexible Electronics and Photonics, Gaithersburg, MD, 2006.

[13] N. P. Suh, Axiomatic Design: Advances and Applications. Oxford University Press, 2001.

[14] D. H. Lee and B. Derby, "Preparation of PZT suspension for direct ink jet printing," Journal of the European Ceramic Society, vol. 24, pp. 1069-1072, 2004

[15] I.W. Hunter and S. Lafontaine, "A comparison of Muscle with Artificial Actuators," Technical Digest of the IEEE Solid State Sensor and Actuator Workshop, Hilton Head, South Carolina, 1992, pp 178-185.

[16] N. Du Toit and S.G. Kim, "Modeling and Design of a MEMS Piezoelectric Vibration Energy Harvester", M.S. Thesis, Massachusetts Institute of Technology, Cambridge MA, 2005.

[17] K. Uchino, *Piezoelectric Actuators and Ultrasonic Motors*. Kluwer Academic Publishers, Boston, 1997 p 79.

[18] K. Yako, H. Kakemoto, T. Tsurumi, and S. Wada, "Doman size dependence of d_{33} piezoelectric properties for barium titanate single crystals with engineered domain configurations," *Materials Science and Engineering B*, vol. 120, pp. 181-185, 2005.

[19] S. Tashiro, T. Murata, K. Ishii, and H. Igarashi, "Grain size Dependence of Third Nonlinear Piezoelectric Coefficient in Lead Zirconate Titanate Ceramics," *Japanese Journal of Applied Physics*, vol. 20, pp. 5679-5682, September 2001.

[20] M. Alguero, B. L. Cheng, F. Guiu, M. J. Reece, M. Poole, N. Alford, "Degradation of the d_{33} piezoelectric coefficient for PZT ceramics under static and cyclic compressive loading," *Journal of the European Ceramic Society*, vol. 21, pp. 1437-1440, 2001.

[21] R. Kremer, A. Boudrioua, P. Moretti, J.C. Loulergue, "Measurements of the non-linear d_{33} of light-ion implanted lithium niobate by second harmonic generation in total reflection geometry," *Optics Communications*, vol. 219, pp. 389-393, February 2003.

[22] R. N. Castellano and L. G. Feinstein, "Ion-beam deposition of thin films of ferroelectric PZT," *J. Appl. Phys.*, vol. 50, 1979, pp. 4406–11.

[23] S. Otsubo *et al*, "Preparation of PZT films by laser ablation", *Japan. J. Appl. Phys.*, vol. 29, 1990, L133–6.

[24] D. Roy , S.B. Krupanidhi and J.P. Dougherty, "Excimer laser ablated lead zirconate titanate thin films," *J. Appl.Phys.*, vol. 69, 1990, pp. 7930–2.

[25] M. Kojima *et al*, "Chemical vapor deposition of PbTiO3 films," *Japan. J. Appl. Phys.*, vol. 22, 1990, pp. 14–17.

[26] B.A. Tuttle *et al*, "Microstructural evolution of PZT thin films prepared by hybrid metallo-organic decomposition," *J. Mater. Res.*, vol. 7, 1992, pp. 1876–82.

[27] G. Spierings *et al*, "Preparation and ferroelectric properties of PZT thin films by spin coating and metalorganic decomposition," *J. Appl. Phys.*, vol. 70, 1992, pp. 2290–8.

[28] P. Murlat, "Ferroelectric Thin Films for micro sensors and actuators: a review" *J. Micromech. Microeng*, vol. 10, 2000, pp. 136-146.

[29] G. J. Willems, Dirk J. Wouters, and H. E. Maes, "Influence of the Pt electrode on the properties of sol-gel PZT films," *Microelectrical Engineering*, vol. 29, pp 217-220, 1995.

[30] S.H. Kim, C.E. Kim, and Y.J. Oh, "Influence of Al_2O_3 diffusion barrier and $PbTiO_3$ seed layer on microstructural and ferroelectric characteristics of PZT thin films by sol-gel spin coating method," *Thin Solid Films*, vol. 305, pp. 321-326, 1997.

[31] R.D. Klissurska, T. Maeder, K.G. Brooks, and N. Setter, "Microstructure of PZT sol-gel films on Pt substrates with different adhesion layers," *Microelectronic Engineering*, vol. 29, pp. 297-300, 1995.

[32] C.L. Dai, F.Y. Xiao, C.Y. Lee, Y.C. Cheng, P.Z. Chang, S.H. Chang, "Thermal effects in PZT: diffusion of titanium and recrystallization of platinum," *Materials Science and Engineering A*, vol. 384, pp. 57-63, May 2004.

[33] J.E. Fromm, IBM J. Res. Dev. 28 (1984) p. 322.

[34] R.D. Deegan, O. Bakajin, T. F. Dupont, G. Huber, S.R. Nagel and T.A. Witten, "Capillary flow as the cause of ring stains from dried liquid drops," *Letters to Nature*, vol. 389, pp. 827-829, October 1997.

[35] C.W. Law, K.Y. Tong, J.H. Li, and K. Li, "Effect of pyrolysis temperature on the characteristics of PZT films deposited by the sol-gel method," *Thin Solid Films*, vol. 335, pp. 220-224, April 1998.

Appendix A.

Ferroelectric Capacitor Masks

Figure A. Pattern for the titanium and platinum bottom electrodes. Wafer outline included for reference only.
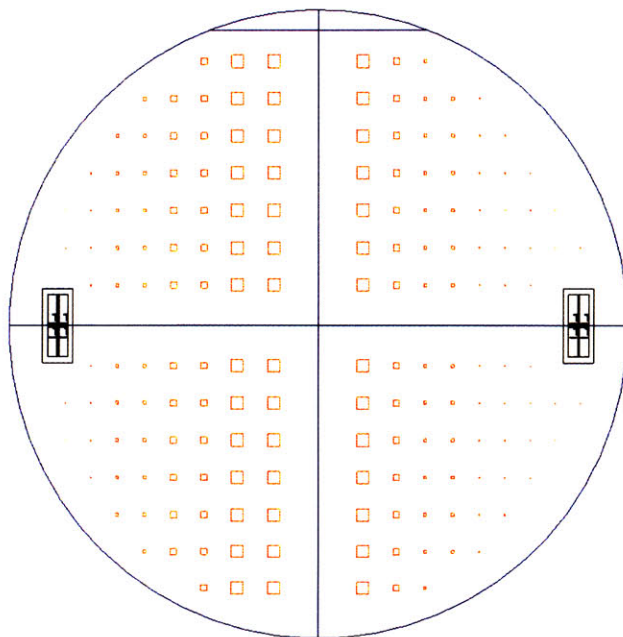
Figure B. Pattern for the poly-silicon PZT wells. This is also a representation of the intended final geometry of the printed PZT layer. Wafer outline included for reference.
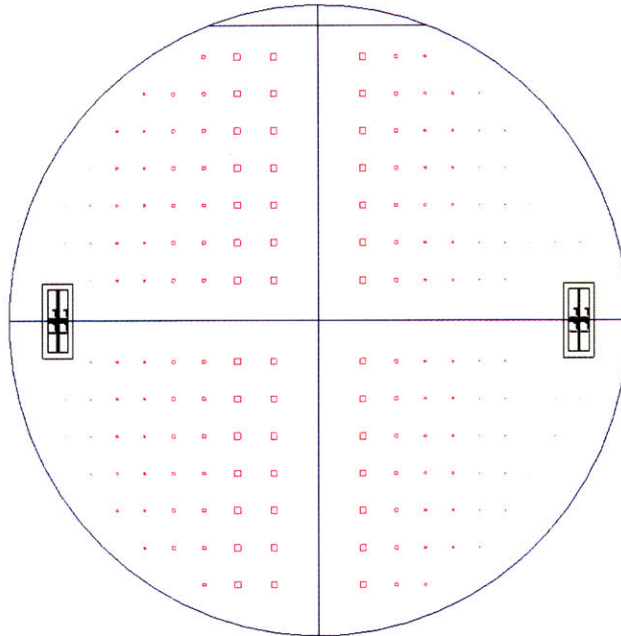
Figure C. Version 1 of the pattern for the platinum top electrodes. Wafer outline included for reference only.
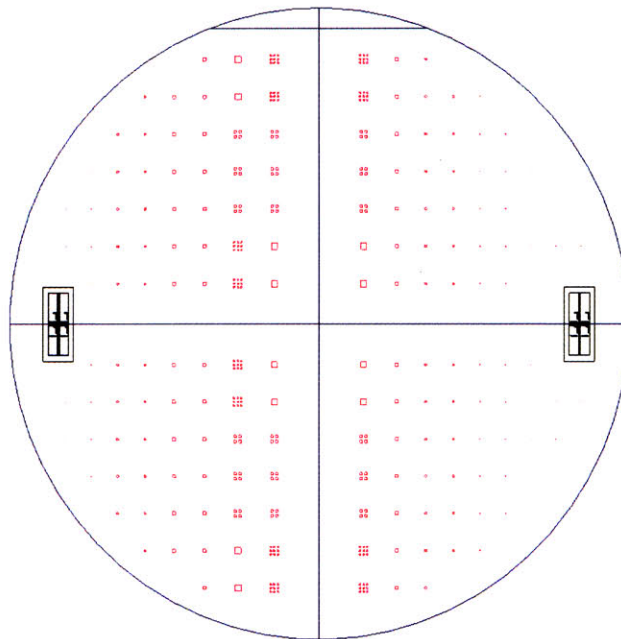
Figure D. Version 2 of the pattern for the platinum top electrodes. Wafer outline included for reference only.

Appendix B.

Ferroelectric Capacitor Process Plans: Part 1

NAME OF PROCESS: Thermal Ink Jet Test Bed Recipe (AZ5214E)

Beginning substrate:
P-type <100> 4" Silicon 1-side polished, 425-475um thickness, TTV<3um, Bow&Wrap<10um, 1-50 Ω-cm

Step 1: **Cleaning of the wafer**
  - RCA cleaning

Step 2: **Thermal Oxide Layer**
  - A2 tube
  - Target deposition 2000A SiO2

Step 3: **Bottom Electrode Deposition and Lift-off**
  Image reversal photo and develop
  - After HMDS, spin coat resist AZ 5214E, recipe: 6sec@0.5krpm, 6sec@0.75krpm, 30sec@4.5krpm to get ~1.8um photoresist.
  - Prebake (30min, 90° C)
  - Expose (EV1 with mask; 1.4sec)
  - Post-bake (30min, 90° C)
  - Flood exposure without mask: (45sec on EV1)
  - Develop – no post-bake required
  - Location: TRL, coater / oven / EV1
  Deposition
  - Target deposition: 200A Ti (Deposition rate: 1A/s) and <500° C substrate temperature
  - Target deposition: 2000A Platinum (Deposition rate: 2A/s)
  - Location: TRL e-beam
  Liftoff
  - Acetone lift-off on electrode; followed by methanol, then DI water, dry with N2 gun

Step 4: **PZT Deposition**
  - PZT deposition will be done in the 5-008 glove box and then transferred back to the TRL for further processing. See attached SOP for transfer procedure.

Step 5: **Top Electrode Deposition and Lift-off**
  Image reversal photo and develop
  - After HMDS, spin coat resist AZ 5214E, recipe: 6sec@0.5krpm, 6sec@0.75krpm, 30sec@4.5krpm to get ~1.8um photoresist.
  - Prebake (30min, 90° C)
  - Expose (EV1 with mask; 1.4sec)
  - Post-bake (30min, 90° C)
  - Flood exposure without mask: (45sec on EV1)
  - Develop – no post-bake required
  - Location: TRL, coater / oven / EV1
  Deposition
  - Target deposition: 200A Ti (Deposition rate: 1A/s) and <500° C substrate temperature
  - Target deposition: 2000A Platinum (Deposition rate: 2A/s)
  - Location: TRL e-beam
  Liftoff
  - Acetone lift-off on electrode; followed by methanol, then DI water, dry with N2 gun

NAME OF PROCESS: Thermal Ink Jet Test Bed Recipe – Polysilicon Wells (AZ5214E)

Beginning substrate:
P-type <100> 4" Silicon 1-side polished, 425-475um thickness, TTV<3um, Bow&Wrap<10um, 1-50 Ω-cm

Step 1: **Cleaning of the wafer**
- RCA cleaning

Step 2: **Thermal Oxide Layer**
- A2 tube
- Target deposition 2000A SiO2

Step 3: **Polysilicon deposition**
- TRL e-beam
- Target deposition 3000A

Step 4: **Pattern and etch of polysilicon**
Image reversal photo and develop
- After HMDS, spin coat resist AZ 5214E, recipe: 6sec@0.5krpm, 6sec@0.75krpm, 30sec@4.5krpm to get ~1.8um photoresist.
- Prebake (30min, 90° C)
- Expose (EV1 with mask; 1.4sec)
- Post-bake (30min, 90° C)
- Flood exposure without mask: (45sec on EV1)
- Develop – no post-bake required
- Location: TRL, coater / oven / EV1
Etching
- 3000A XeF2 isotropic etch
- Location: TRL, XeF2 etcher
Photoresist removal
- O2 plasma, 75min
- Location: TRL, asher

Step 5: **Bottom Electrode Deposition and Lift-off**
Image reversal photo and develop
- After HMDS, spin coat resist AZ 5214E, recipe: 6sec@0.5krpm, 6sec@0.75krpm, 30sec@4.5krpm to get ~1.8um photoresist.
- Prebake (30min, 90° C)
- Expose (EV1 with mask; 1.4sec)
- Post-bake (30min, 90° C)
- Flood exposure without mask: (45sec on EV1)
- Develop – no post-bake required
- Location: TRL, coater / oven / EV1
Deposition
- Target deposition: 200A Ti (Deposition rate: 1A/s) and <500° C substrate temperature
- Target deposition: 2000A Platinum (Deposition rate: 2A/s)
- Location: TRL e-beam
Liftoff
- Acetone lift-off on electrode; followed by methanol, then DI water, dry with N2 gun

Step 6: **PZT Deposition**
- PZT deposition will be done in the 5-008 glove box and then transferred back to the TRL for further processing. See attached SOP for transfer procedure.

Step 7: **Top Electrode Deposition and Lift-off**
Image reversal photo and develop

- After HMDS, spin coat resist AZ 5214E, recipe: 6sec@0.5krpm, 6sec@0.75krpm, 30sec@4.5krpm to get ~1.8um photoresist.
- Prebake (30min, 90° C)
- Expose (EV1 with mask; 1.4sec)
- Post-bake (30min, 90° C)
- Flood exposure without mask: (45sec on EV1)
- Develop – no post-bake required
- Location: TRL, coater / oven / EV1

Deposition
- Target deposition: 200A Ti (Deposition rate: 1A/s) and <500° C substrate temperature
- Target deposition: 2000A Platinum (Deposition rate: 2A/s)
- Location: TRL e-beam

Liftoff
- Acetone lift-off on electrode; followed by methanol, then DI water, dry with N2 gun

Ferroelectric Capacitor Process Plans: Part 2

NAME OF PROCESS: Thermal Ink Jet Test Bed Recipe (NR7)

Beginning substrate:
P-type <100> 4" Silicon 1-side polished, 425-475um thickness, TTV<3um, Bow&Wrap<10um, 1-50 Ω-cm

Step 1: **Cleaning of the wafer**
- RCA cleaning

Step 2: **Thermal Oxide Layer**
- A2 tube
- Target deposition 2000A SiO2

Step 3: **Bottom Electrode Deposition and Lift-off**
Image reversal photo and develop
- After HMDS, spin coat resist NR7, recipe: static dispense ¾ wafer diameter, 6sec@0.75krpm, 30sec@2.5krpm
- Prebake (90sec, 155° C)
- Expose (EV1 with mask; 10sec)
- Post-bake (2min, 120° C)
- Develop in RD6 in shallow beaker, 15-25s, rinse with DI, nitrogen dry
- Location: TRL, coater / oven / EV1

Deposition
- Target deposition: 200A Ti (Deposition rate: 1A/s) and <500° C substrate temperature
- Target deposition: 2000A Platinum (Deposition rate: 2A/s)
- Location: TRL e-beam

Liftoff
- RR4 lift-off on electrode; followed by methanol, then DI water, dry with N2 gun

Step 4: **PZT Deposition**
- PZT deposition will be done in the 5-008 glove box and then transferred back to the TRL for further processing. See attached SOP for transfer procedure.

Step 5: **Top Electrode Deposition and Lift-off**
Image reversal photo and develop
- After HMDS, spin coat resist NR7, recipe: static dispense ¾ wafer diameter, 6sec@0.75krpm, 30sec@2.5krpm

- Prebake (90sec, 155° C)
- Expose (EV1 with mask; 10sec)
- Post-bake (2min, 120° C)
- Develop in RD6 in shallow beaker, 15-25s, rinse with DI, nitrogen dry
- Location: TRL, coater / oven / EV1

Deposition
- Target deposition: 200A Ti (Deposition rate: 1A/s) and <500° C substrate temperature
- Target deposition: 2000A Platinum (Deposition rate: 2A/s)
- Location: TRL e-beam

Liftoff
- RR4 lift-off on electrode; followed by methanol, then DI water, dry with N2 gun

NAME OF PROCESS: Thermal Ink Jet Test Bed Recipe – Polysilicon Wells (NR7)

Beginning substrate:
P-type <100> 4" Silicon 1-side polished, 425-475um thickness, TTV<3um, Bow&Wrap<10um, 1-50 Ω-cm

Step 1: **Cleaning of the wafer**
- RCA cleaning

Step 2: **Thermal Oxide Layer**
- A2 tube
- Target deposition 2000A Si02

Step 3: **Polysilicon deposition**
- TRL e-beam
- Target deposition 3000A

Step 4: **Pattern and etch of polysilicon**
Image reversal photo and develop
- After HMDS, spin coat resist AZ 5214E, recipe: 6sec@0.5krpm, 6sec@0.75krpm, 30sec@4.5krpm to get ~1.8um photoresist.
- Prebake (30min, 90° C)
- Expose (EV1 with mask; 1.4sec)
- Post-bake (30min, 90° C)
- Flood exposure without mask: (45sec on EV1)
- Develop – no post-bake required
- Location: TRL, coater / oven / EV1

Etching
- 3000A XeF2 isotropic etch
- Location: TRL, XeF2 etcher

Photoresist removal
- O2 plasma, 75min
- Location: TRL, asher

Step 5: **Bottom Electrode Deposition and Lift-off**
Image reversal photo and develop
- After HMDS, spin coat resist NR7, recipe: static dispense ¾ wafer diameter, 6sec@0.75krpm, 30sec@2.5krpm
- Prebake (90sec, 155° C)
- Expose (EV1 with mask; 10sec)
- Post-bake (2min, 120° C)
- Develop in RD6 in shallow beaker, 15-25s, rinse with DI, nitrogen dry
- Location: TRL, coater / oven / EV1

Deposition

- Target deposition: 200A Ti (Deposition rate: 1A/s) and <500° C substrate temperature
- Target deposition: 2000A Platinum (Deposition rate: 2A/s)
- Location: TRL e-beam

Liftoff

- RR4 lift-off on electrode; followed by methanol, then DI water, dry with N2 gun

Step 6: **PZT Deposition**

- PZT deposition will be done in the 5-008 glove box and then transferred back to the TRL for further processing. See attached SOP for transfer procedure.

Step 7: **Top Electrode Deposition and Lift-off**

Image reversal photo and develop

- After HMDS, spin coat resist NR7, recipe: static dispense ¾ wafer diameter, 6sec@0.75krpm, 30sec@2.5krpm
- Prebake (90sec, 155° C)
- Expose (EV1 with mask; 10sec)
- Post-bake (2min, 120° C)
- Develop in RD6 in shallow beaker, 15-25s, rinse with DI, nitrogen dry
- Location: TRL, coater / oven / EV1

Deposition

- Target deposition: 200A Ti (Deposition rate: 1A/s) and <500° C substrate temperature
- Target deposition: 2000A Platinum (Deposition rate: 2A/s)
- Location: TRL e-beam

Liftoff

- RR4 lift-off on electrode; followed by methanol, then DI water, dry with N2 gun

Appendix C. Calculations

Because of the wide variation in ink composition, the values chosen for the calculation of the maximum and minimum values of *Bo* and *Z* were based on the maximum and minimum values of the ink components. This is a reasonable approximation for viscosity and density assuming an ideal mixture. Calculating the surface tension of a mixture is more complicated. However, as a first order approximation the values of the solution components will be taken as bounds.

	Viscosity [Pa·S]	Surface Tension [N/m]	Boiling Point [°C]	Density [kg/m^3]
2-Methoxyethaol	1.54E-03	2.80E-02-3.25E-02	125	960-1020
2-Ethlyhexanoic Acid	7.70E-03	2.80E-02	228	905-915
Isopropanol	2.43E-03	2.28E-02	82	785

[ref]

Part 1: Calculation of Bond Number for Film Formation Analysis

$$Bo = \frac{\rho g r^2}{\sigma}$$

From the range of solvent properties, maximum and minimum were used, along with an appropriate range of droplet diameters, to determine the maximum and minimum values of *Bo*.

	Surface Tension [N/m]	Density [kg/m^3]	Droplet Diameter [m]
MIN	2.28E-02	785	5.00E-06
MAX	3.25E-02	1020	1.00E-04

$$Bo_{min} = \frac{785 \cdot 9.8 \cdot (5 \cdot 10^{-6})^2}{3.25 \cdot 10^{-2}} = 5.92 \cdot 10^{-6}$$

$$Bo_{max} = \frac{1020 \cdot 9.8 \cdot (1 \cdot 10^{-4})^2}{2.28 \cdot 10^{-2}} = 4.4 \cdot 10^{-3}$$

Part 2: Calculation of Z for Droplet Dynamic Analysis

$$Z = \frac{(\gamma \rho a)^{1/2}}{\eta} = \frac{Re}{We^{1/2}}$$

From the range of solvent properties, maximum and minimum were used, along with an appropriate range of nozzle diameters, to determine the maximum and minimum values of Z.

	Viscosity [Pa·S]	Surface Tension [N/m]	Density [kg/m^3]	Nozzle Diameter [m]
MIN	1.54E-03	2.28E-02	785	5.00E-06
MAX	7.70E-03	3.25E-02	1020	1.00E-04

$$Z_{min} = \frac{(\gamma \rho a)^{1/2}}{\eta} = \frac{(2.28 \cdot 10^{-2} \cdot 785 \cdot 5 \cdot 10^{-6})^{1/2}}{7.70 \cdot 10^{-3}} = 1.23$$

$$Z_{max} = \frac{(\gamma \rho a)^{1/2}}{\eta} = \frac{(3.25 \cdot 10^{-2} \cdot 1020 \cdot 1 \cdot 10^{-4})^{1/2}}{1.54 \cdot 10^{-3}} = 37.39$$
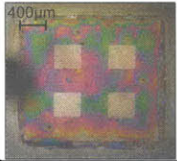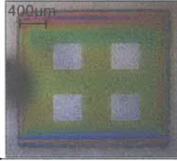
Resistivities:

Peak Voltage During Measurement:	Printed PZT (incomplete pyrolysis – June 2007)	Printed PZT (extended pyrolysis – October 2008)	Spin Coated PZT
5V	$4.5 \cdot 10^{10}$ Ω·cm	$6.4 \cdot 10^{10}$ Ω·cm	
15V	$8.3 \cdot 10^{2}$ Ω·cm	$6.2 \cdot 10^{10}$ Ω·cm	$4.87 \cdot 10^{13}$ Ω·cm [1]

[1] Traina, Zachary J. "A Large Strain Piezoelectric Microactuator by Folding Assembly." MS Thesis, Massachusetts Institute of Technology, 2007. Resistivity of $1 \cdot 10^{11}$ Ω•cm or better is desired as reported: D.L. Polla, L.F. Francis, "Ferroelectric Thin Films in Micro-electromechanical Systems Applications", MRS Bulletin, vol. 21, no. 7, pp 59-65, 1996

Piezoelectric Film Properties (all values are approximate and represent averages of positive and negative values) :

Deposition Type	Deposition Environment	Uniformity	Pyrolysis Time (at 360°C)	Peak Voltage During Measurement [V]	Coercive Field [V]	Saturization Polarization [uC/cm^2]	Remnant Polarization [uC/cm^2]	Picture (if available)
TIJ – June	open air	poor	2 min	19.91	± 3.20	± 7.45	± 5.20	
TIJ - September	class 100 clean room	medium	2 min	19.91	± 4.93	± 8.05	± 5.27	
TIJ - October	class 100 clean room	good (rms ~40nm)	2 hrs	19.91	± 1.90	± 46.15	± 5.40	
Spin Coated	class 100 clean room	excellent	4 min	15	± 3.10	± 43.96	± 21.03	

Appendix E. PZT Ink Development Details

Ink ID	% PZT	% IPA	% EHA	% 2-ME	Oxide % WT	Printable Volume	PZT TIJ Ink Development Notes:
0	100	0	0	0	15.00	180pl, 220pl, 250pl, 280pl	Stable at 220pl, 5 pulses and 2 pulses, glass slide substrate, no thermal treatment; On Pt Cracking and delamination during pyrolysis
1	96	0	4	0	14.40	250pl	More uniform than ink 3, still diffused too much resulting in cracked built up edges
2	75	25	0	0	11.25	250pl	Poor uniformity, some localized cracking. Reduced cracking over Inks 1 and 3.
3	50	0	0	50	7.50	250pl	Excessive diffusion lead to thick film edges which cracked during pyrolysis
4	25	50	25	0	3.75	80pl	Spread too much, formed a splotchy pattern.
5	5	0	0	95	0.75	80pl	Very thin film, poor uniformity
6	10	0	0	90	1.50	80pl	Heavy diffusion, poor uniformity, discontinuous film
7	50	25	10	15	7.50	>80pl	Intermittent Clogging at 80pl; uniformity good, cracking at edges due to excess of diffusion
8	33.3	33.3	0	33.3	5.00	>80pl	Uniformity ok, coverage poor; Clogged at 80pl, no EHA possibly excess ink evaporation
9	31.6	36.6	5	26.6	4.74	80pl	Stable at 80pl, coverage good.
10	30	35	10	25	4.50	80pl	EHA concentration study 1; Splochness after pyrolysis - too much EHA
11	30	35	1	34	4.50	80pl	EHA concentration study 1
12	30	35	0	35	4.50	80pl	EHA concentration study 1
13	30	35	5	30	4.50	80pl	EHA concentration study 1; improved film uniformity, cracking occurred for thicker films

14	15	35	5	45	2.25	35pl	Stable at 35pl, First indication that ME not great; a reduction in concentration but increase in cracking. Too much diffusion
15	15	50	5	30	2.25	35pl	Complete coverage at 70um pitch, uniformity at 50um pitch
16	15	40	4	41	2.25	35pl	Thick areas formed in overlap between printed lines, no quite enough diffusion
17	15	38	8	39	2.25	35pl	Cracking at line edges, too much diffusion
18	15	40	5	40	2.25	35pl	
19	15	50	5	30	2.25	35pl	No cracks during drying; thicker films cracked during pyrolysis
20	15	50	7	28	2.25	35pl	Significant spreading, no cracking
21	30	35	0	35	4.50	35pl	(same as ink 21, intermittent clogging)
22	30	50	4	16	4.50	35pl	cracked during pyroysis
23	15	50	10	25	2.25	35pl	EHA concentration study 2
24	15	50	15	20	2.25	35pl	EHA concentration study 2
25	15	50	12	23	2.25	35pl	EHA concentration study 2
26	15	50	11	24	2.25	35pl	EHA concentration study 2
27	15	50	9	26	2.25	35pl	EHA concentration study 2
28	15	50	8	27	2.25	35pl	EHA concentration study 2
29	15	50	7	28	2.25	35pl	EHA concentration study 2

30	15	50	6	29	2.25	35pl	EHA concentration study 2
31	10	0	6	29	1.50	35pl	EHA concentration study 2
32	15	50	5	30	2.25	35pl	EHA concentration study 2